Smart Materials and Structures

PURPOSE-LED PUBLISHING™

PAPER

Colorless shape memory polyimide films for flexible optoelectronics

To cite this article: Shuting Jiang *et al* 2026 *Smart Mater. Struct.* **35** 115018

View the article online for updates and enhancements.

You may also like

- Tumbling Dice: Radio Constraints on the Presence of Circumstellar Shells around Type Ia Supernovae with Impact Near Maximum Light
Chelsea E. Harris, Laura Chomiuk and Peter. E. Nugent
- An improved point spread function for complex susceptibility-based magnetic particle imaging
Tao Jiang, Wentong Yi, Zhongzhou Du et al.
- Enhanced bone mineralization using hydroxyapatite-based ceramic bone substitute incorporating *Withania somnifera* extracts
Irfan Qayoom, Arun Kumar Teotia, Megha Meena et al.

This content was downloaded from IP address 103.76.86.15 on 13/11/2026 at 06:15

Smart Materials and Structures

Check for updates

RECEIVED
22 July 2026

REVISED
23 September 2026

ACCEPTED FOR PUBLICATION
11 October 2026

PUBLISHED
9 November 2026

PAPER

Colorless shape memory polyimide films for flexible optoelectronics

Shuting Jiang[1], **Deyan Kong**[1,*], **Yu Kang**[1], **Xinli Xiao**[1], **Xiaofei Wang**[2], **Jinsong Leng**[3] and **Yanju Liu**[2,4,*]

[1] MIIT Key Laboratory of Critical Materials Technology for New Energy Conversion and Storage, School of Chemistry and Chemical Engineering, Harbin Institute of Technology, Harbin 150001, People's Republic of China
[2] Suzhou Research Institute, Harbin Institute of Technology, Suzhou 215100, People's Republic of China
[3] National Key Laboratory of Science and Technology on Advanced Composites in Special Environment, Harbin Institute of Technology, Harbin 150080, People's Republic of China
[4] Department of Astronautical Science and Mechanics, Harbin Institute of Technology, Harbin 150001, People's Republic of China
[*] Authors to whom any correspondence should be addressed.

E-mail: dykong@hit.edu.cn and yj_liu@hit.edu.cn

Keywords: colorless, transparent, shape memory polymer, polyimide, high temperature resistance

Supplementary material for this article is available online

Abstract

Transparent polymer substrates for flexible perovskite solar cells and foldable displays must offer high transparency, thermal stability, and active deformability. With the rapid development of intelligent and adaptive flexible electronics, shape memory functionality has emerged as a key requirement for next-generation devices to enable smart behaviors such as self-deployment or morphing. However, although conventional colorless transparent polyimides exhibit outstanding transparency and thermal resistance, they tend to lack shape memory functionality, making it difficult to meet the demands of next-generation intelligent flexible devices such as self-deployable structures. We designed a molecular system using two dianhydrides, one containing a hexafluoroisopropylidene group and one containing ether linkages, and three fluorinated diamines with different rigidities. The hexafluoroisopropylidene and ether units suppress charge-transfer complex formation to enhance optical transparency, while the ether linkages also improve chain flexibility. The varying diamine rigidity enables tuning of thermal properties. Based on this design, colorless shape memory polyimide (co-CSMPI) films were prepared via quaternary copolymerization. The results demonstrate that co-CSMPIs exhibit excellent overall performance. A representative co-CSMPI possesses a glass transition temperature (T_g) of 241 °C, satisfying the requirements for high-temperature processing; a transmittance of 88.0% at 500 nm, indicating good optical transparency. Furthermore, it exhibits excellent shape memory performance, with shape fixity ratios (R_f) of 99.4% and shape recovery ratios (R_r) of 98.9%. The colorless shape memory polyimide films enable lighter device designs, holding great promise for flexible perovskite solar cell substrates and foldable display covers.

1. Introduction

Flexible optoelectronic devices, such as portable energy sources and wearable devices [1–7], have undergone rapid development. Flexible perovskite solar cells have increasingly advanced towards lighter weight and enhanced mechanical flexibility [8–12]. The performance of these flexible optoelectronic devices was highly dependent on colorless transparent substrates [13–18]. Such substrates must possess excellent optical properties, typically requiring a transmittance higher than 85% to ensure high light-harvesting efficiency and display brightness. Simultaneously, they need outstanding thermal stability, generally with a glass transition temperature (T_g) exceeding 200 °C, to withstand the deposition processes of subsequent transparent conductive electrodes and to accommodate the heat generated during long-term device operation [19]. Furthermore, the substrate material should exhibit excellent mechanical properties to

© 2026 IOP Publishing Ltd. All rights, including for text and data mining, AI training, and similar technologies, are reserved.

endure the mechanical stress incurred during repeated bending [20]. Polymer substrates are a promising substrate material for flexible optoelectronics, owing to their advantages such as excellent mechanical flexibility and ultralight weight [21, 22].

Polyimides (PIs), with their exceptional mechanical strength and thermal stability, are commonly used in extreme environments such as aerospace applications, making them ideal candidate materials to address the aforementioned issues [23–27]. However, conventional polyimides exhibit poor transmittance and a yellowish-brown coloration due to the strong charge transfer complexation effect within their molecular backbones, making them less suitable for flexible optoelectronics [28, 29]. To enhance the optical properties of polyimides, researchers commonly inhibit the formation of intense intra/intermolecular charge transfer complexation (CTC) by introducing monomers containing fluorinated groups, alicyclic structures, bulky side groups, or distorted configurations, thereby obtaining colorless transparent polyimide (CPI) films [30–34]. Nevertheless, it remains challenging for current CPI films to achieve a satisfactory balance between thermal and optical properties. For instance, Yi *et al* designed and synthesized three diamine monomers with different alkyl chain lengths, which were then copolymerized with fluorinated monomers. The resulting CPI films exhibited acceptable optical properties ($T400 = 82.9\%$) but suffered from poor thermal performance, with a T_g of only 172.4 °C [35]. Li *et al* synthesized a CPI film with excellent thermal properties ($T_g = 400$ °C) by copolymerizing a synthesized diamine monomer with 4,4′-diaminodiphenylmethane (HPMDA) and an alicyclic dianhydride. However, its optical performance was comparatively inferior ($T400 = 67\%$) [36].

Endowing CPIs with shape memory effect could enable intelligent responsiveness in advanced flexible optoelectronics. Shape memory performance describes a material's ability to recover its permanent shape from a temporary one when triggered by heat, light, electricity, or magnetism [37–41]. Such materials offer advantages including active deformation capability and programmability. Early studies by Xiao *et al* achieved the coexistence of transparency and shape memory in transparent shape memory polyimides, but the T_g was only 171 °C, which is insufficient for high-temperature device processing [38]. Subsequently, Gao *et al* raised the T_g to the 220 °C range while maintaining a transmittance of approximately 86% at 450 nm [42]. Huang *et al* further optimized the thermal performance of CSMPIs to a T_g of 228 °C–250 °C with a transmittance of 80.5%–88.4% at 450 nm [43]. However, these studies mainly reported the performance of a single formulation, and the correlation between copolymer composition and properties—in particular, the use of fluorinated diamines with different rigidities to tune thermal properties—has not been systematically investigated.

In this study, we used dianhydrides bearing hexafluoroisopropylidene and ether linkages to suppress charge transfer for better transparency and flexibility, along with fluorinated diamines of different rigidities to tune thermal properties. From this design, three shape memory polyimide films with high transparency and excellent thermal stability were successfully fabricated via quaternary copolymerization, aiming to broaden their potential applications in flexible optoelectronic devices, including flexible perovskite solar cells and foldable displays.

2. Experimental section

Materials. 4,4′-oxybis [3-(trifluoromethyl)benzenamine] (6FODA, 99.53%), 4,4′-(9 H-fluorene-9,9-diyl); bis(2-fluoroaniline) (FFDA, 99.62%), 2,2′-bis(trifluoromethyl) benzidine (TFMB, 99.98%), 2,2-bis [4-(3,4-dicarboxyphenoxy)phenyl]propane dianhydride (BPADA, 99.00%) and 2,2-bis(3,4-anhydrodicarboxyphenyl) hexafluoropropane (6FDA, 99.98%) were from China Tech (Tianjin) Chemical Co. Ltd and used directly. N, N-dimethylacetamide (DMAC) came from Sinopharm Group Co. Ltd and was further processed by distillation before use.

Preparation of colorless shape memory copolyimide (co-CSMPI) films. First, poly(amic acid) (PAA) solution was synthesized via quaternary copolymerization, followed by thermal imidization to produce co-CSMPI films. The monomer ratios used for these films were summarized in table 1. Additionally, other shape memory polyimides with reduced transparency were prepared by adjusting the monomer molar ratios, as detailed in supplementary table S1.

The synthesis of co-CSMPI-1 was described here as a typical example. A 100 ml three-neck flask was charged with 25 ml of DMAc, 0.2314 g of 6FODA, and 1.2490 g of TFMB. The mixture was stirred under N_2 until completely dissolved. Subsequently, 0.4431 g of 6FDA and 2.0767 g of BPADA were added to the flask. Stirring the mixture under N_2 for 12 h gave the PAA solution. Other co-CSMPI samples were prepared similarly. Figure 1 depicts the polycondensation routes and appearances of co-CSMPI-1, co-CSMPI-2, and co-CSMPI-3.

Table 1. Monomer ratio of the co-CSMPI films.

Sample	Diamine	Dianhydride	Molar ratio of diamine to dianhydride
co-CSMPI-1	6FODA:TFMB = 0.15:0.85	6FDA:BPADA = 0.2:0.8	0.92
co-CSMPI-2	6FODA:FFDA = 0.85:0.15	6FDA:BPADA = 0.2:0.8	0.93
co-CSMPI-3	FFDA:TFMB = 0.3:0.7	6FDA:BPADA = 0.2:0.8	0.95

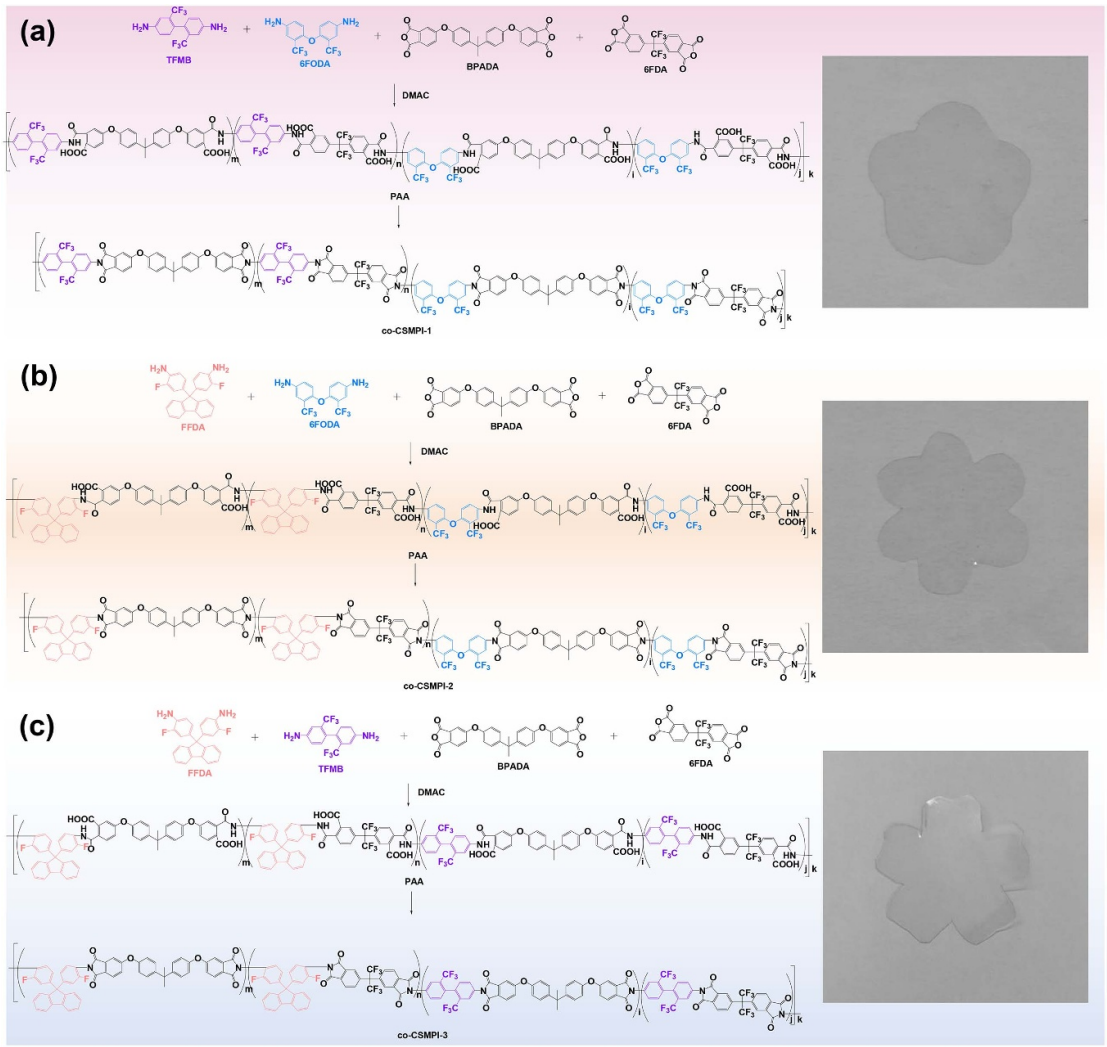


Figure 1. Synthesis routes and corresponding macroscopic appearances of (a) co-CSMPI-1, (b) co-CSMPI-2, and (c) co-CSMPI-3.

The resulting PAA solution was allowed to stand to remove bubbles. After degassing, it was uniformly cast onto a glass plate. The plate was then placed in a vacuum drying oven for stepwise thermal curing according to the following protocol: 80, 120, 150, 180, 210, 240, and finally 280 °C, each held for 2 h. Subsequently, the obtained co-CSMPI films were released from the glass substrate by soaking in water.

Characterization. The molecular structure of the co-CSMPI films was characterized via FT-IR spectrometry over 500–3500 cm^{-1}. The crystal structure of the co-CSMPI films was measured via x-ray diffractometry with Cu Kα radiation at scanning angles of 10° to 60°. The transmittance of the co-CSMPI films was measured by UV–Vis from 300 to 800 nm. The dynamic mechanical properties of the co-CSMPI films were characterized using a dynamic mechanical analyzer under the following conditions: tensile mode under nitrogen, 30 °C–300 °C. The thermal stability of the co-CSMPI films was

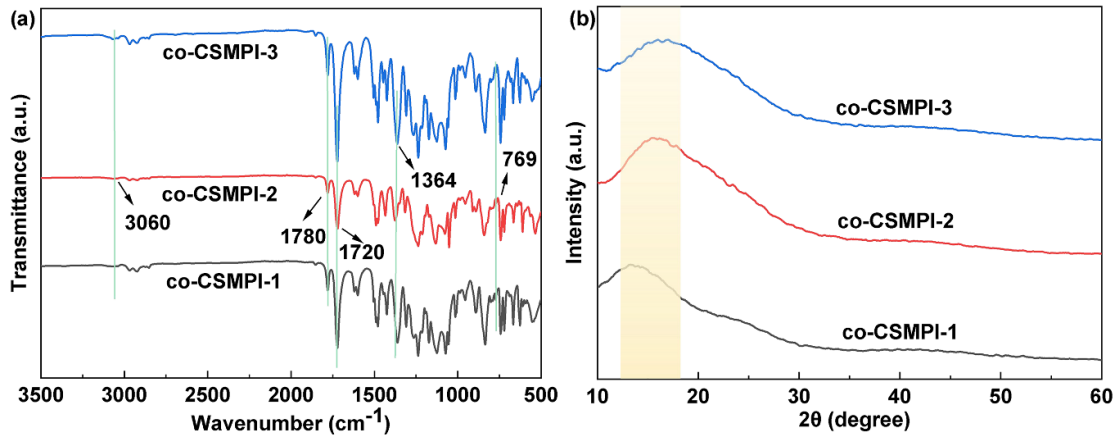


Figure 2. (a) FT-IR and (b) XRD spectra of the co-CSMPI films.

characterized using a thermal analyzer under the following conditions: sample mass of 5–10 mg, nitrogen, 30 °C–800 °C. The mechanical properties of the co-CSMPI films were characterized using an electronic universal testing machine, with specimen dimensions per GB/T 528–2009 and a tensile rate of 5 mm min^{-1}. The co-CSMPI films were cut into dimensions of 10 mm × 30 mm, cleaned, and dried prior to shape memory performance testing. To evaluate the shape memory performance, samples were first heated to T_g + 25 °C on a platform, bent to 180° under external force, and cooled. After removing the force, the bending angle (θ_f) was recorded. The shape recovery was triggered by reheating the samples to T_g + 25 °C, yielding the recovered bending angle (θ_r). The shape fixity ratios (R_f) and shape recovery ratios (R_r) were calculated using the following formulas:

$$R_f = \frac{180^\circ - \theta_f}{180^\circ} \times 100\% \quad (1)$$

$$R_r = \frac{180^\circ - \theta_f}{180^\circ} \times 100\%. \quad (2)$$

3. Results and discussion

Structure of co-CSMPIs. Figure 2(a) shows the FT-IR spectra of the co-CSMPIs. The co-CSMPIs exhibit the stretching vibration peak of the aromatic ring Ar–H at 3060 cm^{-1}, and the polyimide's imide peaks at 1780, 1720, 1364, and 769 cm^{-1}. Among these, the peaks at 1780, 1720, 1364, and 769 cm^{-1} represent imide I (symmetric C=O stretch), imide II (asymmetric C=O stretch), imide III (C–N–C stretch), and imide IV (C–N–C bend), respectively [44]. This indicates that the amide rings of the co-CSMPIs were successfully closed via thermal curing, achieving imidization. Furthermore, no vibration peaks of amino groups were detected in the range of 3300–3500 cm^{-1} for the co-CSMPIs, and no characteristic peaks of PAA were observed at 1660 cm^{-1} (C=O stretching vibration) or 1415 cm (C–N characteristic peak of CONH), confirming that the PAA was completely converted into polyimide, achieving full imidization.

Figure 2(b) shows the XRD patterns, revealing the aggregation state and average molecular chain spacing of the co-CSMPI films. The co-CSMPIs exhibit broad diffraction peaks, indicating their amorphous structure. Furthermore, the diffraction angles (2θ) of co-CSMPI-1, co-CSMPI-2, and co-CSMPI-3 were 13.3058°, 15.3925°, and 17.0291°, respectively. According to the Bragg's law, their average molecular chain spacings (d) were calculated to be 0.6648 nm, 0.5752 nm, and 0.5202 nm, respectively. Large average molecular chain spacings indicate loose chain packing and suppressed interchain interactions. Co-CSMPI-1 shows the largest spacing and co-CSMPI-3 the smallest, a difference arising from the diamine structure, as the dianhydride composition was fixed across the three polymers. 6FODA contains both flexible ether linkages and trifluoromethyl groups. The bulky trifluoromethyl groups push neighboring molecular chains apart in space. Meanwhile, the flexible ether linkages allow these side groups to orient more freely. This further increases the average distance between chains. As a result, 6FODA exhibits the strongest steric hindrance and the loosest molecular chain packing. FFDA contains bulky fluorenyl structures, leading to the most compact molecular chain packing. TFMB has only trifluoromethyl

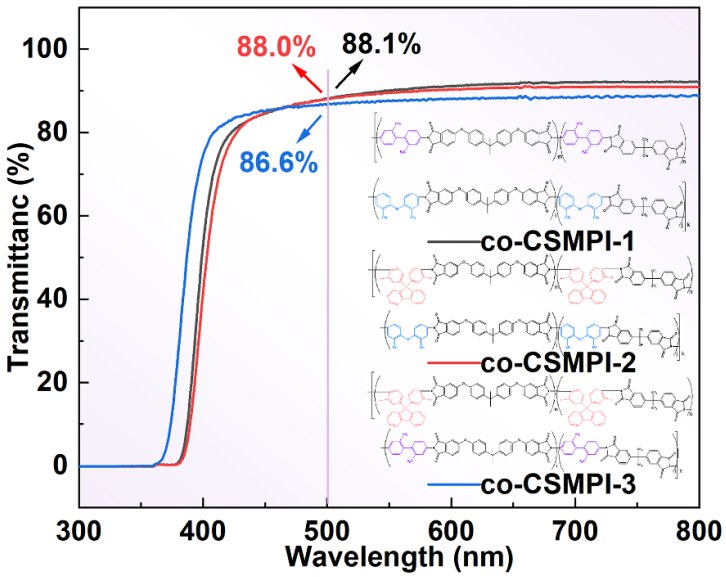


Figure 3. UV–Vis spectrum of the co-CSMPI films.

Table 2. Optical data of the co-CSMPI films.

Name	$\lambda_{cut\text{-}off}$[a] (nm)	T_{500}[b] (%)	T_{avg}[c] (%)
co-CSMPI-1	361	88.1	88.7
co-CSMPI-2	361	88.0	87.7
co-CSMPI-3	360	86.6	87.1

[a] Cut-off wavelength.
[b]Transmittance at 500 nm.
[c]Average transmittance in visible light range (400–780 nm).

groups, and its chain packing density falls between the two. Consequently, co-CSMPI-1, which contains both 6FODA and TFMB, exhibits the largest average molecular chain spacing. Co-CSMPI-3, containing both FFDA and TFMB, shows the smallest average interchain distance. Co-CSMPI-2, containing both FFDA and 6FODA, exhibits an intermediate interchain distance. Therefore, the diamine-controlled molecular chain packing density directly affects charge transfer complex formation, providing a structural basis for the optical transparency of co-CSMPI films [45].

Optical Properties of co-CSMPIs. Figure 1 shows that the co-CSMPI films exhibit a smooth surface and are colorless and transparent. To further investigate the optical performance of the co-CSMPIs, their visible light transmittance was measured, as presented in figure 3, with detailed data listed in table 2. The UV–Vis spectra of the shape memory polyimides with different monomer molar ratios are shown in supplementary figure S1.

For polyimides, optical transparency was closely related to the intramolecular/intermolecular charge transfer complex effect [30], the strength of which depends on the donor–acceptor interaction between diamine and dianhydride and on chain packing density. Through rational molecular structure design, the prepared co-CSMPIs show an average transmittance exceeding 87.1% over 400–780 nm, reflecting excellent optical transparency. This performance arises from the molecular design of monomers, thereby reducing the CTC effect. For the diamines, fluorine atoms or trifluoromethyl groups directly attached to the benzene rings exert a strong inductive effect that suppresses CTC formation. For the dianhydrides, bulky hexafluoroisopropyl or isopropyl groups increase interchain distance and free volume, which further limits CTC interactions.

A comparison of the prepared co-CSMPIs reveals that their visible light transmittance follows the order: co-CSMPI-1 > co-CSMPI-2 > co-CSMPI-3. This order was consistent with the variation trend

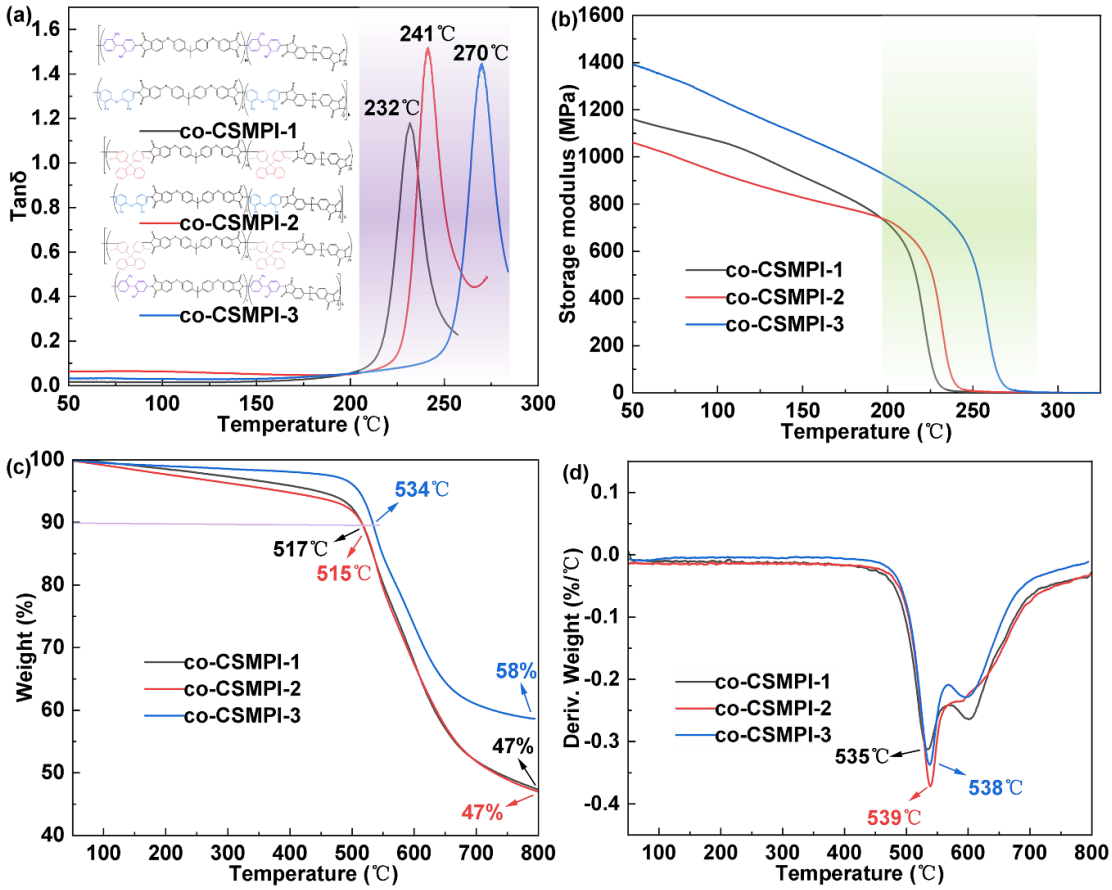


Figure 4. (a) loss factor, (b) storage modulus versus temperature, (c) TGA and (d) DTG of the co-CSMPI films.

of the average molecular chain spacing measured by x-ray diffraction, confirming that a larger inter-chain spacing leads to a weaker intramolecular/intermolecular CTC effect and higher transmittance. The donor–acceptor interaction strength among the three co-CSMPIs depends only on the diamine's electron-donating ability, as they all contain the same dianhydride monomer at the same molar ratio. Specifically, FFDA, containing a bulky conjugated fluorenyl structure, enhances the electron-donating ability of the amino groups. Additionally, its monofluorine atom exhibits a weak electron-withdrawing inductive effect; therefore, FFDA possesses the strongest electron-donating ability. For TFMB, the strongly electron-withdrawing trifluoromethyl group was directly attached next to the amino group, and the molecule lacks electron-donating character. This reduces the electron cloud on the amino nitrogen atom, thus conferring the weakest electron-donating ability. In 6FODA, the ether linkages are electron-donating, while the trifluoromethyl groups are electron-withdrawing; these opposing electronic effects balance each other, resulting in a moderate electron-donating ability. Based on the above analysis, co-CSMPI-1, which contains both 6FODA and TFMB, exhibits the weakest CTC effect between the diamine and dianhydride, leading to the highest transmittance. Conversely, co-CSMPI-3, containing the highest proportion of FFDA, displays the strongest diamine-dianhydride CTC effect, resulting in the lowest transmittance. Co-CSMPI-2, containing two diamines with weaker electron-donating ability but a lower proportion of the weakest donor FFDA than co-CSMPI-3, exhibits an intermediate transmittance. Finally, a lower diamine/dianhydride molar ratio favors chain termination by dianhydride units, thereby reducing diamine end groups that were prone to oxidative yellowing at high temperatures. Consequently, a lower ratio yields higher polyimide film transmittance, as shown in figure S1.

Thermomechanical and thermal properties of co-CSMPIs. The loss factor (tanδ) curves of the co-CSMPIs were presented in figure 4(a). The peak maximum temperature of these curves defines both the T_g and the shape memory transition temperature (T_{trans}) [38]. As shown in figure 4(a), the co-SMPIs exhibit sharp peaks within the temperature range of 200 °C to 300 °C, with the peak maxima located between 232 °C and 270 °C. The T_g values of co-SMPI-1, co-SMPI-2, and co-SMPI-3 were 232 °C, 241 °C, and 270 °C, respectively, reflecting favorable thermomechanical properties imparted by the

Table 3. Thermal property data of the co-CSMPI films.

Name	T_g (°C)	E' at T_g-20 °C (MPa)	E' at $T_g + 20$ °C (MPa)	$T_{10\%}$ (°C)	Rw (%)	$T_{dec,\,max}$ (°C)
co-CSMPI-1	232	600	3	517	47	535
co-CSMPI-2	241	589	4	515	47	539
co-CSMPI-3	270	568	4	534	58	538

rigid aromatic monomers. The glass transition temperature was intrinsically linked to the rigidity or flexibility of the polymer chains; consequently, any factor that diminishes chain flexibility or enhances intermolecular forces will lead to an elevation in T_g. The fluorine/trifluoromethyl groups on the co-CSMPI diamines enable intra- or intermolecular hydrogen bonding. These interactions impede segmental motion, thereby contributing to the increased T_g. The different T_g values of the co-CSMPIs stem from the molecular structures of their diamines. FFDA contains a bulky, rigid fluorenyl group that increases steric hindrance and crosslinking density. This combination restricts segmental motion, making FFDA the most rigid and giving it the highest T_g. In comparison, TFMB possesses a biphenyl structure that imparts considerable local rigidity to the molecular chain. TFMB's rigidity was less pronounced than that of the fluorenyl group, placing its T_g at an intermediate level. Despite some rigidity from 6FODA, its flexible ether linkage acts as a hinge that enhances internal rotation and lowers the activation energy for segmental motion. As a result, 6FODA exhibits the lowest T_g among the three diamines investigated.

The storage modulus (E') curves of the co-CSMPIs were presented in figure 4(b). The E' values of co-SMPI-1, co-SMPI-2, and co-SMPI-3 were 1164 MPa, 1060 MPa, and 1390 MPa, respectively. All samples exhibited a similar trend, with the storage modulus decreasing continuously as the temperature increased. Within their respective glass transition regions (i.e. the T_{trans} region, as seen in the colored regions of the figure), the E' value decreases dramatically, as shown in table 3. This significant modulus drop facilitates the fixation of the temporary shape, thereby endowing the co-CSMPIs with excellent shape memory properties.

The thermogravimetric (TG) curves of the co-CSMPIs and their derivative (DTG) counterparts were shown in figures 4(c) and (d). The temperatures at which 10% weight loss occurs (T_{10}) for co-CSMPI-1, co-CSMPI-2, and co-CSMPI-3 were 517 °C, 515 °C, and 534 °C, respectively, while the residual mass percentages at 800 °C (R_w) were 47%, 47%, and 58%, respectively. The temperature of maximum decomposition rate ($T_{dec,\,max}$) falls within the range of 535 °C–539 °C. At this temperature, rapid decomposition of the aromatic rings, imide rings, and trifluoromethyl groups within the polymer backbone occurs. The results indicate that below 500 °C, the TG curves remain nearly horizontal with minimal weight loss, which is primarily attributable to the evaporation of water and residual solvents, as well as the volatilization of trace small molecules. Consequently, the co-SMPIs decompose slowly below 500 °C, thus meeting the processing requirements of flexible perovskite solar cells. In the temperature range of 500 °C–700 °C, rapid decomposition occurs within the polymer backbone, involving the aromatic rings, imide rings, and trifluoromethyl groups. Even at 800 °C, the co-CSMPIs retain a relatively high residual mass, demonstrating their excellent thermal stability. Notably, the highest FFDA content gives co-CSMPI-3 its superior thermal stability. The rigid conjugated fluorenyl group enhances resistance to thermal decomposition and char formation, while the biphenyl rigidity of TFMB further reinforces the overall chain rigidity. By contrast, the introduction of flexible 6FODA with ether linkages into co-CSMPI-1 and co-CSMPI-2 results in slightly lower thermal stability than that of co-CSMPI-3.

Mechanical properties of co-CSMPIs. Figure 5 shows the stress–strain behavior of the co-CSMPIs. The tensile strength decreases from co-CSMPI-1 to co-CSMPI-3, reflecting that mechanical properties depend on molecular chain structure. Co-CSMPI-1 exhibits the highest tensile strength, which can be primarily attributed to its composition dominated by rigid TFMB, providing excellent load-bearing capacity, supplemented by a small amount of flexible 6FODA that acts as a stress buffer. Energy dissipation from this limited segmental motion prevents the brittle fracture common in purely rigid chains and yields the highest tensile strength. Similarly, co-CSMPI-2 avoids brittle fracture by combining rigid FFDA with flexible 6FODA, yet its tensile strength remains moderate, lower than that of co-CSMPI-1, because of the bulky fluorenyl group. In contrast, co-CSMPI-3, composed of two rigid FFDA and TFMB monomers, might intuitively be expected to exhibit high tensile strength; however, it demonstrates the lowest value.

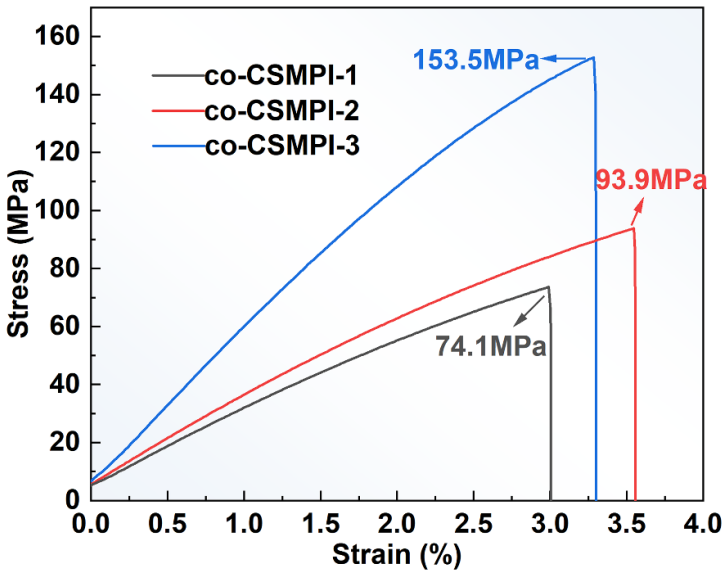


Figure 5. Tensile stress–strain behavior of the co-CSMPI films.

This can be ascribed to structural incompatibility between the two rigid monomers, leading to stress concentration. FFDA's rigid fluorenyl group (fused-ring) and TFMB's linear biphenyl structure create distinct molecular geometries, leading to inhomogeneous chain distribution. Under tension, rigid segments show limited deformation, while interfaces between dissimilar rigid segments become stress concentration points. This facilitates crack initiation and propagation at relatively low strain, ultimately leading to premature brittle failure of the material.

The elongations at break of co-CSMPI-1, co-CSMPI-2, and co-CSMPI-3 were 3.3%, 3.5%, and 3.0%, respectively. The relatively high elongation at break of both co-CSMPI-1 and co-CSMPI-2 stems from their flexible 6FODA component, whose ether linkages promote chain mobility and deformation under stress. Conversely, co-CSMPI-3's fully rigid monomers yield the lowest elongation by restricting chain mobility.

Shape memory of co-CSMPIs. The shape memory performance testing process of the co-CSMPIs was illustrated in figures 6(a)–(c). The results demonstrate that the co-CSMPIs exhibit excellent shape memory properties, with R_f and R_r values of 100% and 99.4% for co-CSMPI-1, 99.4% and 98.9% for co-CSMPI-2, and 99.4% and 98.9% for co-CSMPI-3, respectively. Excellent R_f in the co-CSMPIs stems from the large storage modulus contrast between glassy and rubbery states, while high R_r reflects the abundant aromatic structures that promote chain entanglement and rapid thermal response.

The shape memory mechanism of the co-CSMPIs was schematically illustrated in figure 6(d). Their shape memory behavior was achieved through the synergistic effect of covalent crosslinking networks and dynamic non-covalent interactions [46]. Below T_g, covalent crosslinks form a stable network, while π–π stacking and hydrogen bonds lock segmental motion to fix the permanent shape. Heating above T_g under stress rubberizes the chains, enabling orientation and slippage as non-covalent interactions dissociate, freeing volume for rearrangement. Subsequently, keeping the stress on, cooling below T_g locks the segmental mobility. During this process, π–π stacking and hydrogen bonding were reestablished and stabilized, forming a new conformation through physical crosslinking and enabling the material to acquire a temporary shape. When reheated above T_g, the π–π stacking and hydrogen bonds dissociate again, leading to the disappearance of physical crosslinks. Driven by the recovery stress originating from conformational entropy, the molecular chains spontaneously revert to their initial conformation, ultimately achieving permanent shape recovery.

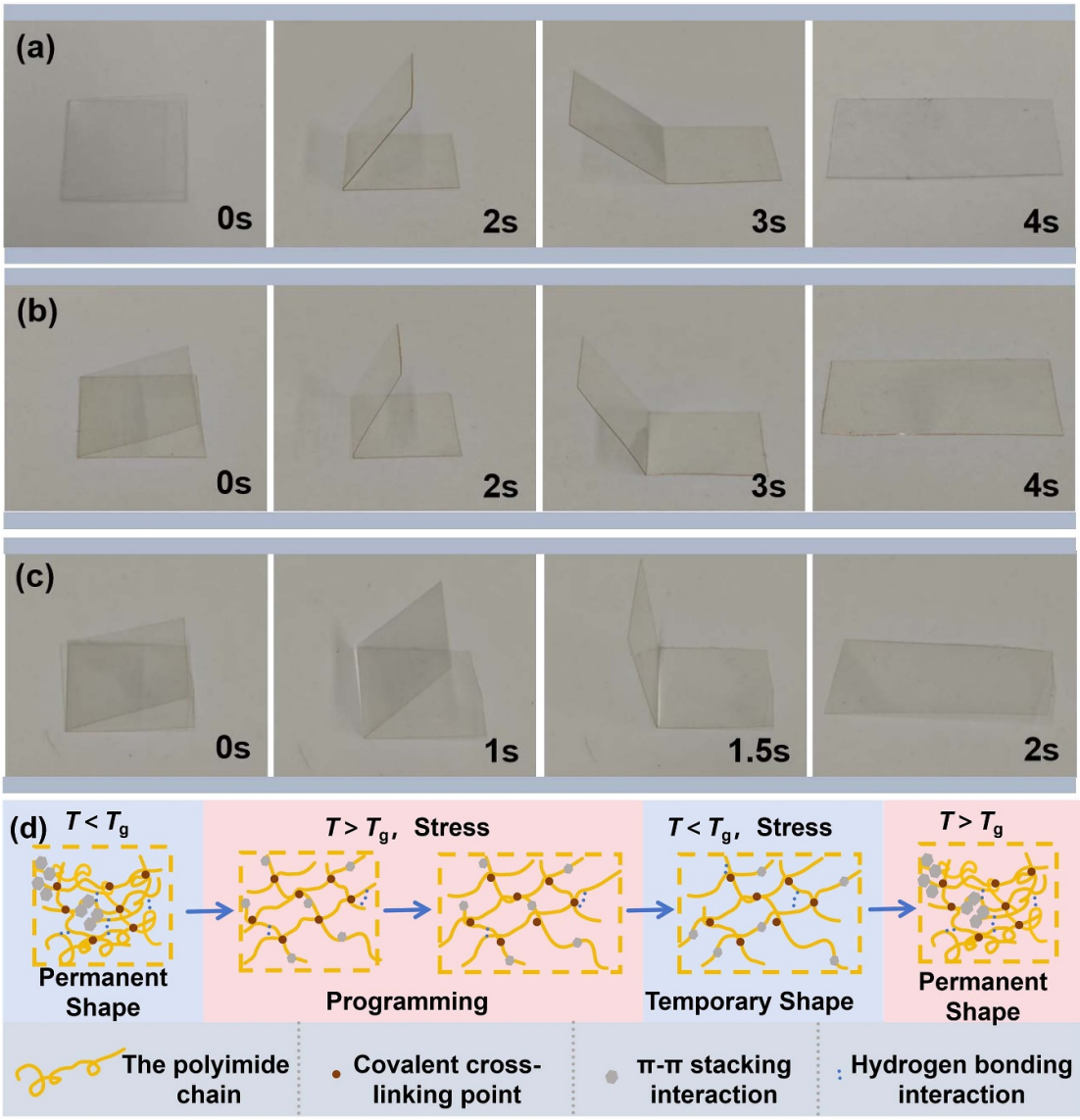


Figure 6. Shape memory processes of (a) co-CSMPI-1, (b) co-CSMPI-2, (c) co-CSMPI-3, and (d) the corresponding mechanism.

4. Conclusions

In summary, through molecular structure design to regulate the copolymer composition, colorless polyimides that combine high transparency, thermal stability, and shape memory characteristics were successfully prepared. The results indicate that a suitable 6FDA/BPADA dianhydride ratio not only preserves the thermal properties of the films but also improves their optical performance. An appropriate ratio of the three diamine monomers not only improves the films' thermal stability but also optimizes their mechanical properties. Among them, co-CSMPI-2 exhibits the best overall performance due to its balanced rigid-flexible structure, achieving a glass transition temperature of 241 °C, a transmittance of 88.0% at 500 nm, a tensile strength of 93.9 MPa, an R_f of 99.4%, and an R_r of 98.9%. These outstanding properties make this series of materials highly promising for applications in high-end flexible optoelectronic devices, such as substrates for flexible perovskite solar cells and cover films for foldable displays.

Acknowledgment

National Natural Science Foundation of China (Granted No. 92271206). Science Foundation of National Key Laboratory of Science and Technology on Advanced Composites in Special Environments (Grant Nos. JCKYS2024603C008, 6142905222910). National Natural Science Foundation of China (Granted No. 12502141).

Data availability statement

All data associated with this study were presented in the paper or the Supporting Information. Additional data sets, materials, and analysis generated during the current study were available from the corresponding authors upon reasonable request.

Author contributions

S J conceived the project idea and designed the experiments, prepared samples, and wrote the manuscript. Y K supported the mechanical analysis. X X and X W contributed to the manuscript check. D K and Y L supervised the entire project. J L managed the entire project.

Conflict of interest

The authors declare no competing financial interest.

ORCID iDs

Shuting Jiang 0009-0004-2561-2289
Yu Kang 0009-0005-9442-6559
Xinli Xiao 0000-0002-3383-2394
Jinsong Leng 0000-0001-5098-9871
Yanju Liu 0000-0001-8269-1594

References

[1] Yang D, Yang R X, Priya S and Liu S Z 2019 Recent advances in flexible perovskite solar cells: fabrication and applications *Angew. Chem., Int. Ed* **58** 4466–83
[2] Shishido H, Sato R, Ieki D, Matsuo D, Saito K, Konagai M and Ishikawa R 2025 High-efficiency perovskite/silicon tandem solar cells with flexibility *Sol. RRL* **9** e2400899
[3] Zhu X J *et al* 2025 Restrictive heterointerfacial delamination in flexible perovskite photovoltaics using a bifacial linker *Adv. Mater.* **37** 2687
[4] Xu Y M, Lin Z H, Wei W, Hao Y, Liu S Z, Ouyang J Y and Chang J J 2022 Recent progress of electrode materials for flexible perovskite solar cells *Nano-Micro Lett.* **14** 117
[5] Kim U, Lee J, Lee Y S and Choi M 2024 Mechanically robust transparent conducting electrodes for flexible perovskite solar cells *Korean J. Chem. Eng.* **41** 3677–92
[6] Wu Y Y *et al* 2023 *In situ* crosslinking-assisted perovskite grain growth for mechanically robust flexible perovskite solar cells with 23.4% efficiency *Joule* **7** 398–415
[7] Xu W Z *et al* 2024 Multifunctional entinostat enhances the mechanical robustness and efficiency of flexible perovskite solar cells and minimodules *Nat. Photon.* **18** 379–87
[8] Lim S Y, Cho I, Hwang H R and Jeong U H 2026 Standardized test method for pure bending evaluation of foldable display materials under natural-arc folding *Microelectron. Reliab.* **178** 116016
[9] Kim M G, Kim Y M and Han S Y 2022 Mechanical reliability prediction of foldable displays using subcritical crack growth in siloxane-based cover window by two-point bending test *Int. J. Precis. Eng. Manuf.* **23** 1301–13
[10] Lee K W, Yi J, Kim M K and Kim D R 2024 Transparent radiative cooling cover window for flexible and foldable electronic displays *Nat. Commun.* **15** 4443
[11] Du Y X, Li Y F, Li C, Xu R, Meng L H and Bai Y P 2025 Optical adhesives and screen sealants for foldable displays: analysis, progress and trends *ACS Appl. Mater. Interfaces* **17** 5578–94
[12] Abbas A, Luo Y J, Ahmad W, Mustaqeem M, Kong L G, Chen J W, Zhou G G, Tabish T A, Zhang Q and Liang Q L 2024 Recent progress, challenges, and opportunities in 2D materials for flexible displays *Nano Today* **56** 102256
[13] Chandrakar A and Khare A 2025 A comprehensive review of flexible perovskite solar cells: materials, mechanisms, properties, applications, and commercialization status *Sol. Energy* **298** 113649
[14] Al-Saleem N K, Al-Naghmaish A, Madani M, Alfawwar W, Elbasiony A M, Alharthi S, Haque M A and Ghobashy M M 2025 Multifunctional roles and advances of polymers in solar cell technologies: a review *RSC Adv.* **15** 35998–6049
[15] Judic M, Lonjon A, Dantras E and Lacabanne C 2024 One-step elaboration of flexible transparent conductive electrodes from silver nanowires/polymer nanocomposites *J. Appl. Polym. Sci.* **141** e55117
[16] Lee J, Kim M S, Jang W and Wang D H 2024 Conductive PEDOT-dominant surface of transparent electrode patch via selective phase transfer for efficient flexible photoelectronic devices *ACS Appl. Mater. Interfaces* **16** 38310–23
[17] Chen C, Liu C, Quan H R, Shi Y L, Han Y, Chai Y, Dong H and Wang J 2025 Inkjet-printed flexible transparent conductive electrodes based on water-soluble sacrificial layer transfer printing technology *J. Electron. Mater.* **54** 5511–9
[18] Ma P, Wang Y, Wang J, Xue L, Lin Y W, Dong Y, Chen P, Du W, Li Y W and Liu B F 2023 Wax-shaped wettability assisted patterning of silver nanowires on various substrates as transparent, flexible, or stretchable electrodes *Appl. Surf. Sci.* **639** 158232

[19] Nakano S, Saito N, Miura K, Sakano T, Ueda T, Sugi K, Yamaguchi H, Amemiya I, Hiramatsu M and Ishida A 2012 Highly reliable a-IGZO TFTs on a plastic substrate for flexible AMOLED displays *J. Soc. Inf. Disp.* **20** 493–8
[20] Kim Y, Song C H, Kwak M G, Ju B K and Kim J W 2015 Flexible touch sensor with finely patterned Ag nanowires buried at the surface of a colorless polyimide film *RSC Adv.* **5** 42500–5
[21] Tang G Q, Zheng F Y, Song J J, Tai Q D, Zhao J and Yan F 2025 Holistic optimization toward ultrathin flexible perovskite solar cells with high efficiency and mechanical robustness *Adv. Sci.* **12** 2415372
[22] Zhu Y B, Li Y C, Li J, Gao J, Lyu Y, Xie J P and Cai H K 2025 Optimizing the perovskite crystal structure for high-efficient flexible perovskite solar cells via ion replacement engineering *J. Mater. Sci., Mater. Electron.* **36** 1505
[23] Daghigh V, Daghigh H and Harrison R 2025 High-temperature polyimide composites-a review on polyimide types, manufacturing, and mechanical and thermal behavior *J. Compos. Sci.* **9** 526
[24] Li L R, Jiang W D, Yang X Z, Meng Y D, Hu P, Huang C and Liu F 2024 From molecular design to practical applications: strategies for enhancing the optical and thermal performance of polyimide films *Polymers* **16** 2315
[25] Hicyilmaz A S and Bedeloglu A C 2021 Applications of polyimide coatings: a review *SN Appl. Sci.* **3** 363
[26] Gouzman I, Grossman E, Verker R, Atar N, Bolker A and Eliaz N 2019 Advances in polyimide-based materials for space applications *Adv. Mater.* **31** 1807738
[27] Ji D Y, Li T, Hu W P and Fuchs H 2019 Recent progress in aromatic polyimide dielectrics for organic electronic devices and circuits *Adv. Mater.* **31** 1806070
[28] Nishihara M, Christiani L, Staykov A and Sasaki K 2014 Experimental and theoretical study of charge-transfer complex hybrid polyimide membranes *J. Polym. Sci. B* **52** 293–8
[29] Lin D L, Liu Y Z, Jia Z Q, Qi S L and Wu D Z 2020 Structural evolution of macromolecular chain during pre-imidization process and its effects on polyimide film properties *J. Phys. Chem. B* **124** 7969–78
[30] Liu Y Y, Wang Y K and Wu D Y 2022 Synthetic strategies for highly transparent and colorless polyimide film *J. Appl. Polym. Sci.* **139** e52604
[31] Matsumoto T 2004 Syntheses of alicyclic polyimides and the optical properties *Kobunshi Ronbunshu* **61** 39–48
[32] Zhang H, Chen L L, Xin H S and Zhang J H 2025 Performance regulation and application evaluation of colorless polyimide for flexible displays *ACS Appl. Mater. Interfaces* **17** 17358–67
[33] Matsumoto T, Ozawa H, Ishiguro E and Komatsu S 2016 Properties of alicyclic polyimides with bis-spironorbomane structure prepared in various solvents *J. Photopolym. Sci. Technol.* **29** 237–42
[34] Xu K, Ke Z, Li D P, Li T, Qian G T, Deng Z Q, Li D D and Yu Y H 2024 Synthesis of novel colorless polyimides from benzimidazole diamines with various linearity *J. Polym. Sci.* **62** 1808–19
[35] Yi D Y, Zuo Z L, Wang K, Pan R C, Chu X M, Li Z, Liu S J and Shang Z H 2025 High transparency and colorless polyimide films derived from aliphatic-chain containing diamine for display technology *Chemistryselect* **10** e05310
[36] Li D W, Li D D, Ke Z, Gu Q, Xu K, Chen C H, Qian G T and Liu G 2023 Synthesis of colorless polyimides with high Tg and low coefficient of thermal expansion from benzimidazole diamine containing biamide *J. Polym. Sci.* **61** 818–28
[37] Ma S Q, Wang S L, Jin S Z, Wang Y Q, Yao G N, Zhao X G and Chen C H 2020 Construction of high-performance, high-temperature shape memory polyimides bearing pyridine and trifluoromethyl group *Polymer* **210** 122972
[38] Xiao X L, Qiu X Y, Kong D Y, Zhang W B, Liu Y J and Leng J S 2016 Optically transparent high temperature shape memory polymers *Soft Matter* **12** 2894–900
[39] Geng M M, Liu T, Zhang X, Xue T T, Fan W and Liu T X 2025 4D printed shape memory polyimide composite aerogels with high recovery stress for load driving *ACS Appl. Mater. Interfaces* **17** 14615–22
[40] Qiu G H, Ma S Q, Wang C B, Zhang D J, Gu Y Y, Zhang J D and Yao J A 2023 Shape memory effect in polyimide-based composites with multiple driving methods *React. Funct. Polym.* **191** 105652
[41] Ma S Q, Zhang K, He H R, Wang S L, Yao J A and Zhao X G 2023 Shape memory polyimides based on different pendant structures *Polym. Test.* **123** 108034
[42] Gao H, Li J R, Liu Y J and Leng J S 2021 Shape memory polymer solar cells with active deformation *Adv. Compos. Hybrid Mater.* **4** 957–65
[43] Huang X Z, Hu R X, Zhang F H, Liu Y J and Leng J S 2023 Transparent shape memory polyimide enables OLED for smart deformation *Compos. A* **175** 107781
[44] Totu E E, Ruse E, Gardea R and Grigorescu A 2008 FT-IR analysis on polyimide selective membranes *Optoelectron. Adv. Mater.* **2** 442–5
[45] Ni H J, Liu J G, Wang Z H and Yang S Y 2015 A review on colorless and optically transparent polyimide films: chemistry, process and engineering applications *J. Ind. Eng. Chem.* **28** 16–27
[46] Li X T, Zhou X Y, Shang R, Xu Q S, Dong J, Zhao X and Zhang Q H 2026 Shape memory polyimides with large strain and high temperature resistance based on covalent-noncovalent dual-crosslinked networks *Adv. Ind. Eng. Polym. Res.* **9** 137–46